Strong Light Absorption of Self-Organized 3-D Nanospike Arrays for Photovoltaic Applications

Rui Yu, Kwong-Lung Ching, Qingfeng Lin, Siu-Fung Leung, Diaz Arcrossito, and Zhiyong Fan*

Department of Electronic and Computer Engineering, Hong Kong University of Science and Technology, Clear Water Bay, Kowloon, Hong Kong SAR, China

ABSTRACT

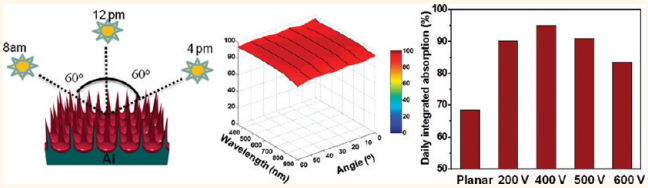

Three-dimensional (3-D) nanostructures have been widely explored for efficient light trapping; however, many of the nanostructure fabrication processes reported have high cost and/or limited scalability. In this work, self-organized 3-D Al nanospike arrays were successfully fabricated on thin Al foils with controlled nanospike geometry such as height and pitch. Thereafter, photovoltaic materials of a-Si and CdTe thin films were conformally deposited on the nanospikes structures thus forming 3-D nanostructures with strong light absorption over a broad wavelength range and photon incident angle. Specifically, 100 nm-thick CdTe film on nanospikes showed 97% peak absorption, and up to 95% day-integrated sunlight absorption. These results indicate that self-organized 3-D Al nanospike arrays can serve as lightweight and low cost substrates for cost-effective thin film photovoltaics.

KEYWORDS: light trapping · aluminum anodization · three-dimensional nanostructures · nanospike · thin film photovoltics

Structural light trapping provides broadband and efficient light absorption enhancement, thus it has been widely utilized to boost the efficiency of bulk photovoltaic (PV) devices. Typically it is realized by texturizing the front surface of a device *via* methods such as chemical etching.[1−4] Nevertheless, because of the limited thickness, it is difficult to apply the same strategy on thin film solar cells. Note that in conventional thin film PV technology, nanotextured transparent conductive oxide (TCO) films are often utilized as front/back contacts to increase light scattering in solar cells; however, increasing the roughness of texturization results in an increase of light absorption in TCO and electrical resistivity.[5,6] In fact, a variety of three-dimensional (3-D) nanostructures, such as arrays of nanowires,[7−9] nanorods,[10−12] and nanopillars,[13−15] *etc.*, have been explored for efficient photon capturing. As an alternative, thin film PV materials can be simply deposited on well-designed 3-D structured substrates for the same purpose. Notably, this approach is even more compatible to the existing thin film PV production processes, therefore, if the 3-D substrates can be fabricated in a cost-effective and scalable fashion they will be quickly adopted by thin film PV industry. Up-to-date, there have been a few attempts to fabricate 3-D substrates for improving PV performance.[16−19] These methods have not achieved sufficient cost-effectiveness and thus still need further development. In this work, we have fabricated arrays of Al nanospike (NSP) on Al foil *via* simple and scalable direct current (DC) anodization under high voltage in conjunction with wet chemical etching. We have observed NSP morphological changes on NSP height, pitch, *etc.*, when the anodization voltage was tuned. In addition, thin film PV materials, including a-Si and CdTe, were deposited on NSP arrays to form 3-D conformal coating. Further optical characterizations have shown that NSP arrays with PV thin films demonstrated much improved optical absorption as opposed to the planar control samples over a large wavelength range and incident angle. Particularly, it was found that with only a 100 nm PV thin film coating, the optimized NSP structure can deliver more than 95% of day-integrated solar irradiance, as compared to ~70% from the planar control sample. These findings have paved the way for developing a novel and practical type of thin film PV module with lightweight, potential flexibility and great cost-effectiveness.

RESULTS AND DISCUSSION

The fabrication process of 3-D Al NSP arrays primarily consists of two steps illustrated in Figure 1a. First, thin Al foils were anodized in diluted citric acid solution

* Address correspondence to eezfan@ust.hk.

Received for review October 6, 2011 and accepted October 23, 2011.

Published online October 23, 2011
10.1021/nn203844z

mixed with ethylene glycol with 200−600 V DC voltage. This anodization step formed an anodic alumina membrane (AAM) on Al substrate with a few micrometer thickness controlled by time (Supporting Information, Figure S1). Thereafter, the AAM layer was chemically etched away in a mixture of phosphoric and chromic acid. The details of anodization and etching can be found in the Methods section. Notably, Al anodization is a low cost and scalable process, thus it has been widely used to fabricate nanostructures, particularly using AAM as templates.[14,20,21] However, such high voltage anodization performed under 200−600 V has rarely been reported before due to the stability of acids. In this work, we have used citric acid as an electrolyte, which has better stability than previously used phosphoric acid.[14,22] More importantly, we have found that mixing ethylene glycol with citric acid can further improve the stability of the electrolyte, thus the anodization voltage can be increased up to 600 V. An additional unique aspect of this work, as opposed to the conventional anodization process, is that the routine electropolishing process was skipped before anodization. It not only simplified the fabrication process, but more importantly it was found that the unpolished Al substrates yielded much better NSP array uniformity as compared to those that were electropolished, and the mechanism will be discussed in detail later.

Figure 1 panels b−e show the 60° tilted-angle-view scanning electron microscopy (SEM) images of Al substrates anodized at the voltages of 200, 400, 500, and 600 V, respectively. It can be clearly seen that there is a morphological transition while increasing the voltage. Specifically, 200 V anodized Al demonstrates an array of dimples replicating the shape of the bottom of the AAM, as shown in Figure 1b. These dimples show local hexagonal ordering with a domain size of ~2 μm due to the self-organizing effect during AAM pore growth.[23] However, only a few NSP can be found on the substrate with less than 1 μm height. In contrast, Al substrates anodized with 400 V (Figure 1c) and 500 V (Figure 1d) have shown uniformly high density of NSPs on the surface, with height ~3 μm. However, when the anodization voltage was increased up to 600 V (Figure 2e), the surface morphology appears to be similar to that anodized with 200 V, except that the size of the dimples is much larger and there is no obvious local hexagonal ordering found.

Apparently, both nanodimples and NSPs are the replica of AAM structures from the bottom. Therefore, the average pitch of the dimples and NSPs is controlled by anodization voltages, which roughly follows the relationship of 2.5 nm/V as it can be easily seen from Figure 1b−e.[24] Thus the average pitches of NSP arrays for 400 and 500 V anodization are 1 and 1.3 μm, respectively. On the other hand, the fact that 400 and 500 V anodization produces NSP arrays is intriguing. In

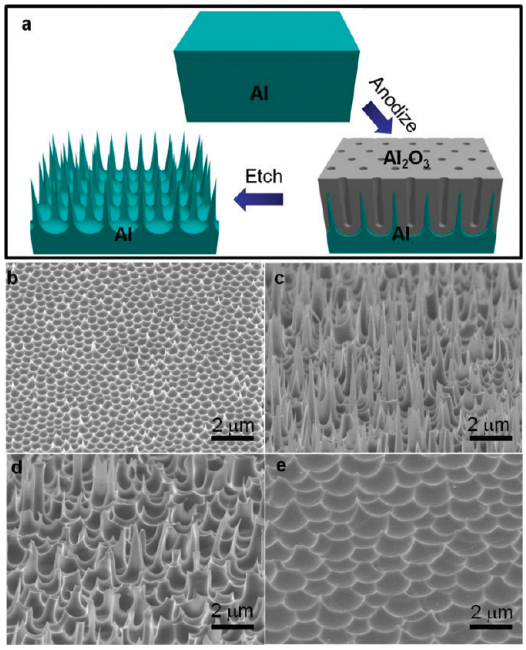

Figure 1. (a) Schematic of the anodization and etching process to fabricate 3D Al NSP arrays (not drawn to scale). SEM images of 3D Al NSP arrays anodized at the voltages of (b) 200, (c) 400, (d) 500, (e) 600 V at a tilted angle of 60°.

fact, it was found that 450 V anodization also yielded NSP arrays (Supporting Information, Figure S2a) thus it is believed that there is a voltage range of 400−500 V leading to NSP arrays formation. As formation of high density uniform arrays of NSP on Al surface by anodization has not yet been reported, systematic experiments were performed to identify the NSP formation mechanism in this work. It is well-known that AAMs prepared by electrochemical oxidation in acidic electrolytes are composed of closely packed alumina nanotubes.[24] Because of volumetric expansion caused by anodization, there exists a repulsive force among these alumina nanotubes, leading to self-organized hexagonal nanotube arrays with no gaps among them.[23,25] However, in our experiment, the bottom of AAMs showed a loosely packaged nanotube array structure with many visible voids, particularly for 400−500 V anodization, as shown in Figure 2a. These voids inevitably led to formation of Al NSPs which were embedded in the AAM, as evident in the inset of Figure 2a. However, we have found that anodization of electropolished smooth Al substrates could not form high density arrays of NSP (Supporting Information, Figure S2b). And the resulting bottom of an AAM shown in Figure 2b demonstrates a more closely packed structure as compared to that anodized on unpolished Al substrates in Figure 2a. Consistently, it was not easy to observe NSPs embedded in AAMs, as shown in the inset of Figure 2b.

In the past, uniform arrays of NSPs have not been achieved mainly because such a high voltage anodization has rarely been performed and Al substrates were

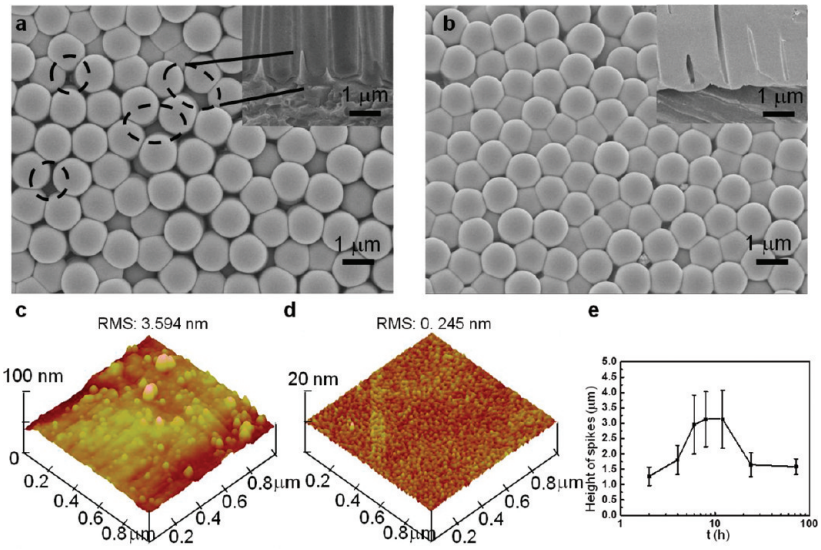

Figure 2. SEM images of the bottom of alumina cylinders using (a) unpolished Al and (b) polished Al anodized at 400 V for 9 h. Holes circled in (a) are originally filled with Al NSPs. Insets are the cross section images of the corresponding alumina without etching of aluminum, clearly showing the existence of Al NSPs embedded in the AAM cylinders. (c) 3D AFM images of surface of unpolished Al and (d) polished Al substrate. (e) Height of Al NSPs as a function of anodization time anodized under 400 V.

conventionally always electropolished before anodization. High voltage anodization leads to large diameter alumina nanotubes with higher mechanical strength as compared to those prepared by low voltage anodization; this can potentially lead to difficulty of self-organization into a hexagonal close-pack structure, causing appearance of voids among alumina nanotubes. On the other hand, to investigate the difference between unpolished and polished Al substrates, atomic force microscopy (AFM) was performed on these substrates, and the results are shown in Figure 2c,d. It is evident that the unpolished Al surface has over 10× surface roughness than the polished one, measured by morphology root-mean-square (rms). It is known that in the beginning stage of AAM growth, Al surface defects have a concentrated electric field leading to formation of initial pores.[23,26] Therefore, a large number of random defects on the unpolished Al surfaces can cause significantly more ununiform growth of the pores than on the polished Al surfaces, leading to a large number of voids between neighboring nanotubes.[27] During AAMs growth, these voids are filled with Al, thus Al NSPs will be observed after etching away AAMs. Notably, following the above rationale, the height of the NSPs will shrink when the AAM growth time is prolonged, due to the self-organizing mechanism improving the ordering of alumina nanotubes. In fact, this has been confirmed by the measurements of NSP height for Al samples anodized with different times ranging from 2 to 72 h. As shown in Figure 2e, NSP height increases for anodization times from 2 to 9 h with a peak average of 3 μm, mainly due to increase of AAM thickness. However, if the anodization time is longer than 9 h, NSP height decreases monotonically over the time down to about 1 μm at 72 h. In short, formation of NSP arrays on anodized Al surfaces is attributed to a combinational effect of high anodization voltage and an excessive amount of random defects on unpolished Al surfaces. In addition, the fact that 600 V-anodized Al samples have short NSP is not contradictory to the above explanation. This observation can be simply ascribed to the extremely slow growth rate of AAM under 600 V due to the utilization of low electrolyte concentration at low temperature to sustain a stable anodization (Supporting Information, Figure S1).

As it has been mentioned previously, the 3-D Al NSP arrays fabrication process is highly scalable. In our work, though the typical size of samples is ~1 cm^2, we have successfully fabricated uniform NSP arrays on Al with an area as large as 7 × 6.5 cm^2 (Supporting Information, Figure S3), which was simply limited by the size of our reaction container. Considering the fact that 3-D nanostructures have excellent photon capturing capability, such a low-cost and scalable process is highly attractive for cost-effective photovoltaics. To further explore the potency of the 3-D NSP arrays for PV applications, we have deposited thin films of PV materials including a-Si and CdTe, *via* plasma-enhanced chemical vapor deposition (PECVD) and thermal chemical vapor deposition (CVD) methods. Figure 3 panels a and b demonstrate 60° tilted angle view of NSP arrays coated with 100 nm a-Si and CdTe films, respectively. And the insets are images with higher magnification. It can be seen that both a-Si and CdTe thin films were conformally deposited on Al NSPs, and the CdTe film shows polycrystalline structures with grain size 50−100 nm.

The as-prepared 400 V Al NSP samples appear to be white color with diffuse reflection, indicating strong

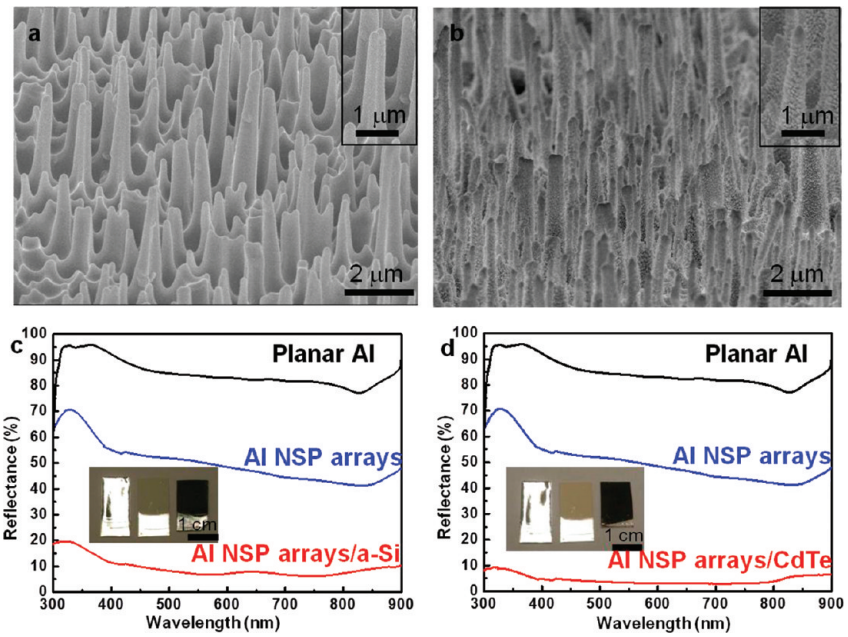

Figure 3. SEM images of Al NSP arrays substrate anodized at 400 V deposited with (a) a-Si, (b) CdTe at a tilted angle of 60°. Insets of panels a and b are a single Al NSP coated with corresponding light absorbers. Optical reflectance of Al substrates deposited with (c) a-Si, (d) CdTe. Insets are the optical images of the corresponding samples, from left to right: planar Al, Al NSP arrays (anodized at 400 V), and a-Si- or CdTe-coated Al NSP arrays.

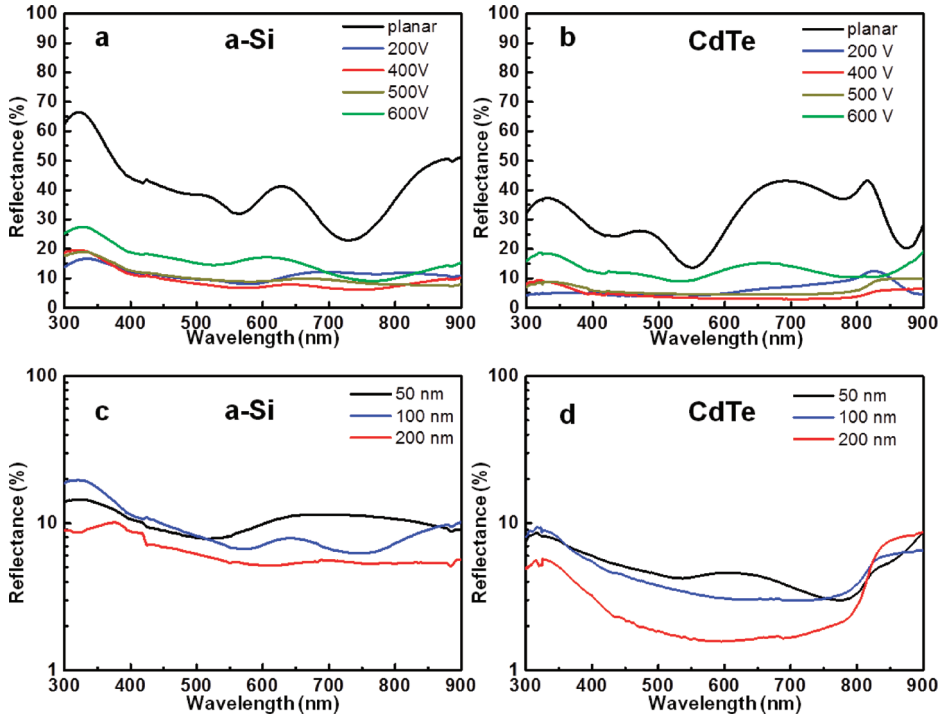

Figure 4. Reflectance spectra of 3D Al NSP arrays deposited with 100 nm (a) a-Si, (b) CdTe. Reflectance spectra of Al NSP arrays deposited with different thickness of (c) a-Si, (d) CdTe (normal incidence).

light scattering in NSP structures. As a comparison, a fresh Al substrate cleaned with electropolishing appears to be mirror-like with specular reflection. However, after coating a-Si and CdTe, the Al NSP samples turned into black color with very low reflectance, as shown in the inset of Figure 3 panels c and d. To further characterize optical properties of a-Si and CdTe coated NSP arrays, their optical reflectance was measured with ultraviolet−visible (UV−vis) spectroscopy equipped with an integrating sphere, together with clean and polished Al and as-prepared Al NSPs with no coating for comparison. As shown in Figure 3c,d, the clean and planar Al substrate has a reflectance of 80−95% over a broad range of wavelengths (300−900 nm), while the

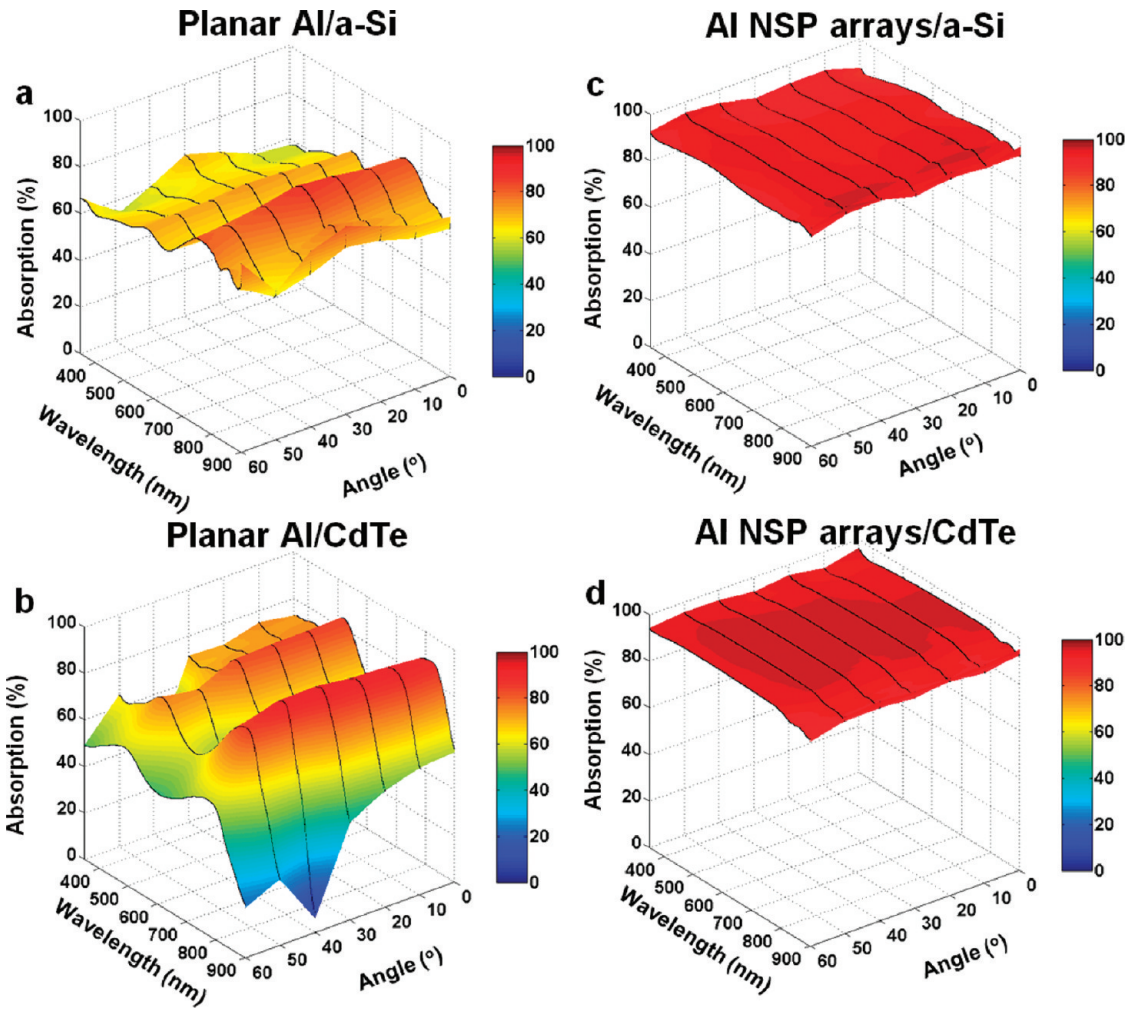

Figure 5. Angular and wavelength dependent absorption spectra of 3D Al NSP arrays deposited with 100 nm (a) a-Si on planar Al, (b) a-Si on Al NSP arrays, (c) CdTe on planar Al, and (d) CdTe on Al NSP arrays substrate.

as-prepared Al NSP sample has lower reflectance down to 40−70%. In clear contrast, the a-Si- and CdTe-coated NSP samples have much lower reflectance. Specifically, a 100 nm a-Si-coated NSP sample shows a reflectance of 5−20% (Figure 3c), and a 100 nm CdTe-coated NSP sample shows a reflectance of 3−10%, with below 5% reflectance for the 400−800 nm wavelength.

Low reflectance of the a-Si- and CdTe-coated NSP arrays indicates a strong light trapping effect in the structures. In many studies such a light trapping effect was also explained with a gradual change of effective refractive index when photons enter the structure from air.[28,29] In this regard, the ununiform height of the NSPs results in a smoother transition of effective refractive index from air, as compared to the case where the NSPs have uniform height. To shed light on the effect of PV thin film thickness, and the geometrical factors, reflectance spectra of NSP arrays prepared with different anodization voltages and NSP arrays coated with different PV film thicknesses were obtained, as shown in Figure 4. Specifically, Figure 4a shows the reflectance spectra of NSP arrays prepared with voltages of 200, 400, 500, and 600 V. In this study 100 nm thick a-Si was deposited on the structures with PECVD. For the sake of comparison, a polished planar Al sample was also deposited with 100 nm a-Si and measured at the same time. It is evident that all the anodized samples have much lower reflectance than the planar control sample among which the 400 V NSP arrays sample give the lowest reflectance over the most part of the wavelength range. Figure 4b shows the similar trend for 100 nm CdTe film-coated samples. These observations are consistent with the SEM images in Figure 1b−e, showing that the 400 V NSP arrays have the best density and uniformity. To investigate the effect of PV film thickness on light trapping, 50, 100, and 200 nm of a-Si and CdTe films were deposited on 400 V NSP samples, and the reflectance spectra are shown in Figure 4c,d. In general, the overall reflectance reduces with an increase of film thickness. Particularly, 200 nm CdTe-coated 400 V NSP arrays show close to only 1% reflectance, over a broad range of spectrum, indicating close to 99% light absorption.

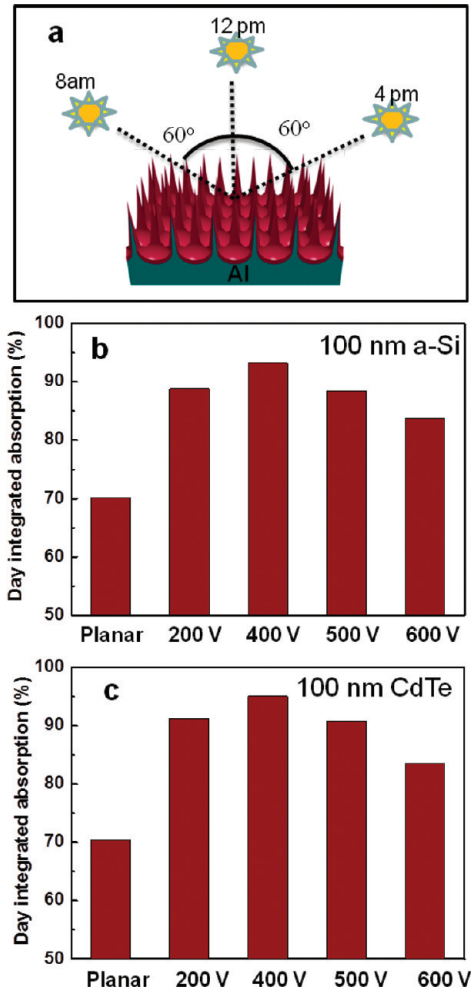

Figure 6. (a) Schematic of angular-dependent absorption calculation. (b) Day integrated absorption of same thickness of a-Si and (c) CdTe on different Al NSP arrays substrates.

The results shown above suggest PV material coated NSP arrays are excellent photon harvesting structures. In fact, although there have been many reports on nanowire and nanopillar light trapping structures with uniform diameters, the unique tapered shape of an NSP creates a gradual change of effective refractive index of the entire 3-D structure, which greatly reduces the reflectance of the structure, similar to the case of nanoneedles, nanocones, and nanotips.[28−31] Therefore, as compared to planar thin film PV devices, much thinner materials are required for sufficient light absorption on NSP structures. A thinner light absorber is beneficial for many nano/microcrystalline thin film PV devices due to the shortened minority carrier migration path and improved carrier collection efficiency.[14] Particularly for a-Si PV, using thinner a-Si can mitigate the Staebler−Wronski effect associated performance degradation.[32,33] Besides improving photon capturing and carrier collection capabilities, additional advantages of Al NSP arrays for thin film PV rest in the fact that Al has been widely used for low cost and stable back contact of solar cells; thus Al NSP together with Al substrate can serve as an excellent bottom contact conveniently.[34−36] And thin Al foils not only are lightweight materials but also have certain flexibility, enabling portable and flexible PV applications.

Notably, the above optical measurements were all performed with normal incident light, for practical PV applications, light absorption from angular incidence has to be considered simply due to the change of solar angle over the time in a day. Therefore, we have characterized the angular absorption property of 400 V anodized NSP arrays and planar Al substrates coated with both 100 nm a-Si and CdTe films with an integrating sphere schematically shown in Supporting Information, Figure S4. Specifically, the light incident angle was tuned from 0° to 60° with 10° interval, and a full spectral reflectance curve was obtained in each step. Thereafter, absorption spectra were calculated simply by subtracting reflectance since there was no transmission. As clearly shown in Figure 5a,b, both of the planar a-Si and CdTe samples show low absorption with oscillating features that originate from thin film interference. In contrast, both a-Si and CdTe NSP samples demonstrate much higher absorption with small dependence on angle and wavelength (Figure 5c,d). Particularly, the CdTe NSP sample shows above 95% absorption over the entire angle range for the 400−800 nm wavelength. In addition, the angular dependent measurements were also performed on Al NSP arrays prepared at other voltages including 200, 500, and 600 V, for both a-Si (Supporting Information, Figure S5) and CdTe (Figure S6). It is worth noting that Figure 4 panels a and b show that the 400 V NSP sample has just slightly lower reflectance overall than the 200 V NSP sample measured with normal incident light, though their surface morphologies appear to be drastically different (Figure 1b,c). However, the angular dependent measurements demonstrate that the absorption of 200 V NSP samples decreases pronouncedly with increase of incident light angle (Supporting Informatioin, Figure S5b and Figure S6b). This observation can be explained by the fact that the 400 V NSP samples have much more pronounced 3-D structures on the surfaces, as compared to 200 V NSP samples, thus photons coming from different angles can be more efficiently trapped in the structures.

Following the angular dependent absorption measurements, we have performed day-integrated solar energy absorption analysis, by integrating the absorption spectra with AM1.5 solar irradiance spectrum in the range of 300−900 nm (Supporting Information). As shown in Figure 6a, 60° incident angle corresponds to 4 h before and after noon time, assuming that the sample and the sun are confined within the equatorial plane with the sample facing the sun at noon. Figure 6b shows the day-integrated absorption of 100 nm a-Si on different types of substrates, showing 93% absorption for 400 V NSP arrays, while only 70% for the planar

control sample. Meanwhile, Figure 6c shows that 400 V NSP arrays coated with 100 nm CdTe can absorb 95% of light over the 8 h period of a day, as opposed to only 70% for the planar control sample. Note that although 500 V NSP arrays have much higher surface structures than 200 V NSP arrays, their day-integrated absorptions are almost the same. This can be explained by the fact that the 200 V NSP arrays have an average pitch of 500 nm (Figure 1b), which matches well with the optical wavelength at the irradiance peak of the solar spectrum.[37] However, the average pitch of 500 V NSPs is $\sim$1 μm (Figure 1d), thus the light trapping effect is not significant for a short wavelength. This rationale can be extended to 600 V NSP arrays which have even larger NSP pitch and lower absorption, and it is also consistent with reflectance measurements shown in Figure 4a,b, in which 500 V NSP arrays have a lower reflectance to long wavelength than 200 V NSP arrays, but a higher reflectance at short wavelength. These results have shown that the 3-D NSP arrays are promising PV structures with broad band and broad angle light absorption capability which can be tuned largely with nanostructure engineering.

CONCLUSION

In summary, we have demonstrated fabrication of 3-D Al NSP arrays with controlled NSP height and pitch. As the uniform arrays of NSPs produced by self-organized anodization approach have rarely been reported before, their formation mechanism was investigated and discussed, revealing a combinational effect of high voltage and high density of random defects on starting Al surface. Thereafter, we have performed systematic studies on optical reflectance/absorption of the NSP arrays after conformally coating with a-Si and CdTe films, suggesting strong and broad band optical absorption with small angle dependence. In the end, we have shown that NSP arrays coated with thin film PV materials can achieve up to 94% day-integrated sunlight, in 300−900 nm wavelength range. Combining with the fact that the NSP fabrication process has low-cost merit with excellent scalability, these unique NSP structures are highly attractive for cost-effective thin film PV applications.

METHODS

3-D Al NSP Arrays Preparation. Self-organized Al NSP arrays were fabricated using the following process. Aluminum foils (99.5% purity) of thickness 0.25 mm were cut into 1 cm by 2 cm pieces, then cleaned with acetone followed by rinsing with IPA and deionized water. Then the Al chips were placed in a home-built anodization setup. Anodization was carried out in a mixture of citric acid, ethylene glycol, and phosphoric acid. The applied voltages were in the range of 200−600 V bias while the time ranged from 9 to 16 h. For the 200 V voltage, the solution contained 2 wt % citric acid, ethylene glycol, and 85 wt % phosphoric acid in the ratio of 200:100:0.5 v/v%; for the 400 V $\sim$500 V voltages, the solution was 2:1 v/v% for the 2 wt % citric acid and ethylene glycol; while for 600 V voltage, the solution was diluted to 1:1 v/v% for the 2 wt % citric acid and ethylene glycol. Carbon rod was used as the counter-electrode. For the exposure of 3D Al NSP arrays, the AAM film was etched in a mixture of chromium acid (1.5 wt %) and phosphoric acid (6 wt %) solutions at 63 °C for 1 h. After etching, the 3-D Al NSP array chips were cleaned with DI-water and blown dry with air for the subsequent thin film deposition. For the exposure of the cross-section of AAM, the Al layer is selectively etched using saturated $CuCl_2$ solution.

a-Si and CdTe Preparation. The growth of a-Si on Al NSP arrays were carried out in a STS 310PC PECVD system. SiH_4 (25 s.c.c.m.) was used as the reactant and He (1182 s.c.c.m.) was used as the transport gas. To grow 100 nm a-Si on different Al substrates, different growth time was carried out ranging from 18−24 min. The growth of CdTe on Al NSP arrays were performed in a 1 in. quartz tube furnace with two resistive heating zones, constituting the chemical vapor deposition (CVD) method. H_2 (5 s.c.c.m.) was used as the transport gas with a chamber pressure of 22 mTorr. The temperatures of the source zone and sample zone were 700 and 150 °C, respectively. After 50 min of growth, the furnace was turned off and allowed to cool down naturally.

Structural and Optical Characterization. The microstructure of the samples was examined using field-emission scanning electron microscopy (FE-SEM, JSM-6700F). The optical properties were investigated by reflectance measurements (UV−vis−IR spectrometer, Lambda 20, Perkin-Elmer) performed at room temperature. Angular-dependent reflection measurements were carried out with a custom-built 5 in. integrating sphere apparatus (Supporting Information, Figure S4). A Xenon lamp was used as the light source to provide a wide range of wavelengths (λ = 200−1100 nm), which was monitored by a spectrometer.

Acknowledgment. This work was partially supported by DAG09/10.EG09, HKUST Research Project Competition Grant (RPC11EG38), and National Research Foundation of Korea funded by the Korean Government (NRF-2010-220-D00060).

Supporting Information Available: AAM thickness *versus* anodization time is shown in Figure S1, SEM images of Al NSPs anodized at 450 V and Al NSPs anodized at 400 V using polished Al are given in Figure S2, optical image of a large chip of Al NSP arrays is shown in Figure S3, schematic of integrating sphere measurement and illustration of the illumination conditions are given in Figure S4, and angular and wavelength dependent absorption spectra of 3D Al NSP arrays deposited with 100 nm a-Si and CdTe are shown in Figure S5 and Figure S6, separately. This material is available free of charge *via* the Internet at http://pubs.acs.org.

REFERENCES AND NOTES

1. Muller, J.; Rech, B.; Springer, J.; Vanecek, M. TCO and Light Trapping in Silicon Thin Film Solar Cells. *Sol. Energy* **2004**, *77*, 917–930.
2. Nayak, B. K.; Iyengar, V. V.; Gupta, M. C. Efficient Light Trapping in Silicon Solar Cells by Ultrafast-Laser-Induced Self-Assembled Micro/Nano Structures. *Prog. Photovolt: Res. Appl.* **2011**, *19*, 631–639.
3. Koynov, S.; Brandt, M. S.; Stutzmann, M. Black Nonreflecting Silicon Surfaces for Solar Cells. *Appl. Phys. Lett.* **2006**, *88*, 203107.
4. Schirone, L.; Sotgiu, G.; Califano, F. P. Chemically Etched Porous Silicon as an Anti-reflection Coating for High Efficiency Solar Cells. *Thin Solid Films* **1997**, *297*, 296–298.
5. Krc, J.; Smole, F.; Topic, M. Potential of Light Trapping in Microcrystalline Silicon Solar Cells with Textured Substrates. *Prog. Photovolt: Res. Appl.* **2003**, *11*, 429–436.
6. Shah, A. V.; Schade, H.; Vanecek, M.; Meier, J.; Vallat-Sauvain, E.; Wyrsch, N.; Kroll, U.; Droz, C.; Bailat, J. Thin-

Film Silicon Solar Cell Technology. *Prog. Photovolt: Res. Appl.* **2004**, *12*, 113–142.
7. Garnett, E.; Yang, P. Light Trapping in Silicon Nanowire Solar Cells. *Nano Lett.* **2010**, *10*, 1082–1087.
8. Chang, H.; Lai, K.; Dai, Y.; Wang, H.; Lin, C.; He, J. Nanowire Arrays with Controlled Structure Profiles for Maximizing Optical Collection Efficiency. *Energy Environ. Sci.* **2011**, *4*, 2863–2869.
9. Kelzenberg, M. D.; Boettcher, S. W.; Petykiewicz, J. A.; Turner-Evans, D.; Putnam, M. C.; Warren, E. L.; Spurgeon, J. M.; Briggs, R. M.; Lewis, N. S.; Atwater, H. A. Enhanced Absorption and Carrier Collection in Si Wire Arrays for Photovoltaic Applications. *Nat. Mater.* **2010**, *9*, 239–244.
10. Han, S. E.; Chen, G. Toward the Lambertian Limit of Light Trapping in Thin Nanostructured Silicon Solar Cells. *Nano Lett.* **2010**, *10*, 4692–4696.
11. Wang, X.; Pey, K. L.; Yip, C. H.; Fitzgerald, E. A.; Antoniadis, D. A. Vertically Arrayed Si Nanowire/Nanorod-Based Core−Shell pn Junction Solar Cells. *J. Appl. Phys.* **2010**, *108*, 124303.
12. Tang, Y. B.; Chen, Z. H.; Song, H. S.; Lee, C. S.; Cong, H. T.; Cheng, H. M.; Zhang, W. J.; Bello, I.; Lee, S. T. Vertically Aligned p-Type Single-Crystalline GaN Nanorod Arrays on n-Type Si for Heterojunction Photovoltaic Cells. *Nano Lett.* **2008**, *8*, 4191–4195.
13. Wang, H.; Lai, K.; Lin, Y.; Lin, C.; He, J. Periodic Si Nanopillar Arrays Fabricated by Colloidal Lithography and Catalytic Etching for Broadband and Omnidirectional Elimination of Fresnel Reflection. *Langmuir* **2010**, *26*, 12855–12858.
14. Fan, Z.; Razavi, H.; Do, J.; Moriwaki, A.; Ergen, O.; Chueh, Y.; Leu, P. W.; Ho, J. C.; Takahashi, T.; Reichertz, L. A.; Neale, S.; Yu, K.; Wu, M.; Ager, J. W.; Javey, A. Three-Dimensional Nanopillar-Array Photovoltaics on Low-Cost and Flexible Substrates. *Nat. Mater.* **2009**, *8*, 648–653.
15. Naureen, S.; Sanatinia, R.; Shahid, N.; Anand, S. High Optical Quality InP-Based Nanopillars Fabricated by a Top-Down Approach. *Nano Lett.*, published online September 26, 2011, http://pubs.acs.org/doi/full/10.1021/nl202628m.
16. Zhu, J.; Hsu, C.; Yu, Z.; Fan, S.; Cui, Y. Nanodome Solar Cells with Efficient Light Management and Self-Cleaning. *Nano Lett.* **2010**, *10*, 1979–1984.
17. Vanecek, M.; Babchenko, O.; Purkrt, A.; Holovsky, J.; Neykova, N.; Poruba, A.; Remes, Z.; Meier, J.; Kroll, U. Nanostructured Three-Dimensional Thin Film Silicon Solar Cells with Very High Efficiency Potential. *Appl. Phys. Lett.* **2011**, *98*, 163503.
18. Camacho, R. E.; Morgan, A. R.; Flores, M. C.; McLeod, T. A.; Kumsomboone, V. S.; Mordecai, B. J.; Bhattacharjea, R.; Tong, W.; Wagner, B. K.; Flicker, J. D. Carbon Nanotube Arrays for Photovoltaic Applications. *J. Miner. Met. Mater. Soc.* **2007**, *59*, 39–42.
19. Paudel, T.; Rybczynski, J.; Gao, Y. T.; Lan, Y. C.; Peng, Y.; Kempa, K.; Naughton, M. J.; Ren, Z. F. Nanocoax Solar Cells Based on Aligned Multiwalled Carbon Nanotube Arrays. *Phys. Status Solidi A* **2011**, *208*, 924–927.
20. Lee, M. H.; Lim, N.; Ruebusch, D. J.; Jamshidi, A.; Kapadia, R.; Lee, R.; Seok, T. J.; Takei, K.; Cho, K. Y.; Fan, Z.; Jang, H.; Wu, M.; Cho, G.; Javey, A. Roll-To-Roll Anodization and Etching of Aluminum Foils for High-Throughput Surface Nanotexturing. *Nano Lett.* **2011**, *11*, 3425–3430.
21. Fan, Z.; Kapadia, R.; Leu, P. W.; Zhang, X.; Chueh, Y.; Takei, K.; Yu, K.; Jamshidi, A.; Rathore, A. A.; Ruebusch, D. J.; Wu, M.; Javey, A. Ordered Arrays of Dual-Diameter Nanopillars for Maximized Optical Absorption. *Nano Lett.* **2010**, *10*, 3823–3827.
22. Chu, S. Z.; Wada, K.; Inoue, S.; Isogai, M.; Katsuta, Y.; Yasumori, A. Large-Scale Fabrication of Ordered Nanoporous Alumina Films with Arbitrary Pore Intervals by Critical-Potential Anodization. *J. Electrochem. Soc.* **2006**, *153*, B384–B391.
23. Jessensky, O.; Muller, F.; Gosele, U. Self-Organized Formation of Hexagonal Pore Arrays in Anodic Alumina. *Appl. Phys. Lett.* **1998**, *72*, 1173–1175.
24. Lee, W.; Ji, R.; Gosele, U.; Nielsch, K. Fast Fabrication of Long-Range Ordered Porous Alumina Membranes by Hard Anodization. *Nat. Mater.* **2006**, *5*, 741–747.
25. Chu, S. Z.; Wada, K.; Inoue, S.; Isogai, M.; Yasumori, A. Fabrication of Ideally Ordered Nanoporous Alumina Films and Integrated Alumina Nanotubule Arrays by High-Field Anodization. *Adv. Mater.* **2005**, *17*, 2115–2119.
26. Zhao, S.; Chan, K.; Yelon, A.; Veres, T. Novel Structure of AAO Film Fabricated by Constant Current Anodization. *Adv. Mater.* **2007**, *19*, 3004–3007.
27. Lee, W.; Nielsch, K.; Gösele, U. Self-Ordering Behavior of Nanoporous Anodic Aluminum Oxide (AAO) in Malonic Acid Anodization. *Nanotechnology* **2007**, *18*, 475713.
28. Zhu, J.; Yu, Z.; Burkhard, G. F.; Hsu, C. M.; Connor, S. T.; Xu, Y.; Wang, Q.; McGehee, M.; Fan, S.; Cui, Y. Optical Absorption Enhancement in Amorphous Silicon Nanowire and Nanocone Arrays. *Nano Lett.* **2008**, *9*, 279–282.
29. Chueh, Y. L.; Fan, Z.; Takei, K.; Ko, H.; Kapadia, R.; Rathore, A. A.; Miller, N.; Yu, K.; Wu, M.; Haller, E. E. Black Ge Based on Crystalline/Amorphous Core/Shell Nanoneedle Arrays. *Nano Lett.* **2009**, *10*, 520–523.
30. Yeh, L. K.; Lai, K. Y.; Lin, G. J.; Fu, P. H.; Chang, H. C.; Lin, C. A.; He, H., Jr. Giant Efficiency Enhancement of GaAs Solar Cells with Graded Antireflection Layers Based on Syringelike ZnO Nanorod Arrays. *Adv. Energy Mater.* **2011**, *1*, 506–510.
31. Liu, C. H.; Chen, C. H.; Chen, S. Y.; Yen, Y. T.; Kuo, W. C.; Juang, J. Y.; Liao, Y. K.; Kuo, H. C.; Lai, C. H.; Chen, L. J. Large Scale Single-Crystal Cu (In, Ga) Se_2 Nanotip Arrays for High Efficiency Solar Cell. *Nano Lett.* **2011**, *11*, 4443–4448.
32. Battaglia, C.; Escarré, J.; Söderström, K.; Erni, L.; Ding, L.; Bugnon, G.; Billet, A.; Boccard, M.; Barraud, L.; De Wolf, S. Nanoimprint Lithography for High-Efficiency Thin-Film Silicon Solar Cells. *Nano Lett.* **2011**, *11*, 661–665.
33. Staebler, D. L.; Wronski, C. R. Reversible Conductivity Changes in Discharge-Produced Amorphous Si. *Appl. Phys. Lett.* **1977**, *31*, 292–294.
34. Sun, B.; Findikoglu, A. T.; Sykora, M.; Werder, D. J.; Klimov, V. I. Hybrid Photovoltaics Based on Semiconductor Nanocrystals and Amorphous Silicon. *Nano Lett.* **2009**, *9*, 1235–1241.
35. Nath, M.; Chatterjee, P.; Damon-Lacoste, J.; Roca i Cabarrocas, P. Criteria For Improved Open-Circuit Voltage in a-Si: H(N)/c-Si(P) Front Heterojunction with Intrinsic Thin Layer Solar Cells. *J. Appl. Phys.* **2008**, *103*, 034506.
36. Barrio, R.; Gandia, J. J.; Carabe, J.; Gonzalez, N.; Torres, I.; Munoz, D.; Voz, C. Surface Recombination Analysis in Silicon−Heterojunction Solar Cells. *Sol. Energy Mater. Sol. Cells* **2010**, *94*, 282–286.
37. Nelson, J., Ed. In *The Physics of Solar Cells*; Imperial College Press: London, 2003.